Materials for Quantum Technology



**PAPER** • **OPEN ACCESS**

# Nitrogen-vacancy centers in diamond: discovery of additional electronic states

To cite this article: Minh Tuan Luu *et al* 2024 *Mater. Quantum. Technol.* **4** 035201

IOP Publishing Mater. Quantum Technol. 4 (2024) 035201 https://doi.org/10.1088/2633-4356/ad61b3

Materials for Quantum Technology



OPEN ACCESS

RECEIVED
9 April 2024

REVISED
6 June 2024

ACCEPTED FOR PUBLICATION
10 July 2024

PUBLISHED
19 July 2024



PAPER

# Nitrogen-vacancy centers in diamond: discovery of additional electronic states

**Minh Tuan Luu**[1], **Ali Tayefeh Younesi**[1] **and Ronald Ulbricht**[*]

Max-Planck Institut für Polymerforschung, Ackermannweg 10, 55128 Mainz, Germany
[1] Both authors contributed equally.
[*] Author to whom any correspondence should be addressed.

**E-mail:** ulbricht@mpip-mainz.mpg.de

**Keywords:** ultrafast spectroscopy, color centers in diamond, electronic structure

Supplementary material for this article is available online

## Abstract

Nitrogen-vacancy (NV) defect centers in diamond are key to applications in quantum sensing and quantum computing. They create localized electronic states in the diamond lattice with distinct population relaxation pathways following photoexcitation that ultimately enable its unique properties. The defect is known to exist in two charge states: neutral and negative, with respectively one and two known optically-active electronic transitions. Here, we report on the observation of a large number of hitherto undiscovered excited electronic states in both charge states as evidenced by distinct optical transitions in the infrared to ultraviolet part of the spectrum. These transitions are observed by monitoring the electronic relaxation of NV centers after photoexcitation using transient absorption spectroscopy, directly probing transient phenomena occurring on timescales from femtoseconds to microseconds. We also for the first time probed the electron transfer dynamics from the $^3E$ state of $NV^-$ to nearby single-substitutional nitrogen defects ($N_s$) that leads to the well-known effect of NV photoluminescence quenching.

Nitrogen-vacancy (NV) centers have seen rising popularity in advanced quantum sensing applications [1, 2]. NV centers have two charge states, neutral ($NV^0$) and negatively-charged ($NV^-$), where $NV^0$ features one known optical transition with a zero-phonon line (ZPL) at 2.15 eV and $NV^-$ two transitions at 1.95 eV and at 1.19 eV, respectively (figure 1(a)). Ensembles of NV also contain single-substitutional nitrogen defects ($N_s$), where the relative concentration of both defects determines the equilibrium NV charge state distribution [3, 4]. When the NV concentration approaches the $N_s$ concentration, more $NV^0$ appears in equilibrium, whereas only $NV^-$ is present when $N_s \gg NV$. All relevant application scenarios are based on $NV^-$, whose key feature is the spin polarization cycle established by photoexcitation that involves a series of spin-state selective relaxation channels that preferentially populate the $m_s = 0$ level of $^3A_2$, see figure 1(a). This relaxation sequence in turn enables optically-detected magnetic resonance (ODMR) through detection of the photoluminescence (PL) contrast. The spin polarization can be manipulated by either applying resonant microwave (MW) or large transverse magnetic fields.

Decades of research on NV centers have made them one of the best-understood solid-state defects. Yet, large gaps remain in our understanding of the electronic structure and the processes determining key features [5]. For instance, some predicted electronic states have not been observed yet, including localized NV states [6, 7] and the recently proposed bound-exciton Rydberg states of $NV^0$ [8]. Not only is our understanding of electronic excited states essential for furthering the performance of existing applications, such as improving the photoionization contrast in photocurrent-based NV magnetometry [9, 10]. It is also key to inspiring new scientific directions and technological applications, for instance related to the aforementioned Rydberg states of $NV^0$. The influence of $N_s$ on NV properties remains to be fully characterized: the presence of $N_s$ is known to lower the NV spin contrast and quench PL by providing non-radiative decay channels, most likely via electron tunneling from $^3E$ to $N_s$ [11, 12]. A proper characterization of this process could potentially aid in mitigating effects that are detrimental to

performance. Most spectroscopic techniques employed in the field probe material properties in a (quasi-)steady state. Additional information can be obtained by driving the system out of equilibrium by photoexcitation and monitoring the relaxation dynamics, for instance using pulsed laser excitation and (transient) PL detection [13, 14]. While these methods can provide useful data on specific decay channels, they generally rely on detecting radiative relaxation processes, thus missing non-radiative channels such as the aforementioned electron tunneling [15]. Furthermore, these methods do not provide the broad spectral coverage and sufficient time resolution that would be required to observe short-lived excited state transitions that can lie anywhere from the infrared (IR) to the ultraviolet (UV) part of the spectrum.

Here, we use transient absorption (TA) spectroscopy to probe all relevant NV electronic transitions on timescales from femtoseconds to microseconds after photoexcitation, thereby establishing a complete picture of the photoexcitation dynamics of NV centers by following the population relaxation pathways [16, 17]. We use a range of bulk diamond substrates containing NV centers in the few-ppm range, with $N_s$ concentrations ranging from few to 180 ppm. This permits measuring both NV charge states and assessing the influence of $N_s$ concentration. We observe hitherto undiscovered excited state transitions for NVs in both charge states, which, in the case of $NV^0$, are comprised of resonances with both Lorentzian and Fano lineshapes, suggesting an intricate mix of localized defect excitations and bound-to-continuum transitions.

## 1. Results

### 1.1. Intrinsic dynamics of $NV^-$

To characterize the dynamics of $NV^-$ centers, we choose a $NV^0$-free sample (sample S5, see supplementary figure 4 and table 1) and perform TA measurements with a 150 fs pump pulse at 515 nm at sample temperature of 10 K (figure 1(a)). After relaxation within the NV phonon sideband (PSB) occurring on sub-ps timescales [18, 19], all subsequent dynamics are related to electronic relaxation processes. We measure the pump-induced change of the transmission of a broadband white-light (WL) pulse in a spectrally-resolved fashion as a function of pump-probe delay and express the measured quantity as the normalized differential transmission $\Delta T/T$ (supplementary section 1.1). A $\Delta T/T$ spectrum at pump-probe delay of 4 ns is shown in figure 1(b). One observes positive $\Delta T/T$ contributions of the triplet transition $^3A_2$-$^3E$ from ground-state bleaching (GSB, resembling absorption) of the ZPL at 1.95 eV and its PSB, which is due to the fact that excitation reduces the ground state population in $^3A_2$ and thus the absorption. One can also observe stimulated emission (SE, resembling PL) to the red side of the ZPL originating from excited state population in $^3E$, as well as absorption ($\Delta T/T < 0$) from the singlet transition $^1E \rightarrow {}^1A_1$ at 1.19 eV (with PSB). The latter absorption feature arises, since in the NV ensemble, $^1A_1$ is already partially populated after 4 ns. Also visible is an absorptive feature of the $^2E \rightarrow {}^2A_2$ transition at 2.15 eV, indicating pump-induced population of $NV^0$ in its ground state $^2E$, broad excited state absorption (ESA) from $^3E$ to the CB on the blue side of the spectrum, and an ESA peak at 2.38 eV.

The ISC relaxation channel can be best monitored by transiently probing the singlet absorption at 1.19 eV (figure 1(c)). The rise time of ≈10 ns is determined by the $^3E \rightarrow {}^1A_1 \rightarrow {}^1E$ transition time. Since $^1A_1 \rightarrow {}^1E$ is ≈100 ps [20], and thus much faster than $^3E \rightarrow {}^1A_1$, we can assume the absorption rise to be equivalent to the $^3E \rightarrow {}^1A_1$ ISC time. The subsequent decay reveals the $^1E \rightarrow {}^3A_2$ dynamics (supplementary figures 8 and 9). We plot the absorption transient with and without the presence of a strong permanent magnet placed close to the sample. In the former case, the spin polarization in $^3A_2$ is scrambled due to the large transverse magnetic field, hence steering the relaxation towards the ISC decay channel, increasing the TA signal amplitude at 1.19 eV. This effect is akin to applying a CW microwave field resonant with the $m_s = 0 \rightarrow \pm 1$ transition at ≈2.9 GHz. The peak amplitude difference of both measurements is thus the spin contrast. The temperature dependence of the extracted ISC times shown in the upper inset agrees well with previous reports [13, 14, 21]. The lower inset shows the dependence of the $^3E \rightarrow {}^1A_1$ ISC time on $N_s$ concentration. One can clearly observe a decrease with increasing $N_s$ concentration, a well-known effect that is accompanied by a reduction of the $^3E \rightarrow {}^3A_2$ PL lifetime and quantum yield. This reduction is believed to be caused by electron transfer from $^3E$ to nearby $N_s$ acting as a non-radiative decay channel that quenches PL and reduces the PL lifetime and spin contrast [11, 22]. We will later present TA measurements that probe the dynamics of this electron transfer process.

As mentioned before, we also observe an ESA resonance at 2.38 eV, see TA spectrum at 2 ps time delay shown in figure 1(d). The inset shows a baseline-corrected enlarged version, where one can observe a series of broader peaks to the red side of the ZPL. The inset also shows fits to the peaks using appropriate models and the numbers indicate their energetic distance to the ZPL in meV (supplementary section 2.1.1). The broader linewidth of these peaks and their energetic distance to the ZPL suggest them being vibronic modes of the 2.38 eV transition that produce a feature-rich PSB. The ESA feature decays with the same dynamics as the relevant $^3A_2 \leftrightarrow {}^3E$ transitions, confirming it being an excited state of $NV^-$. We do not observe any signs

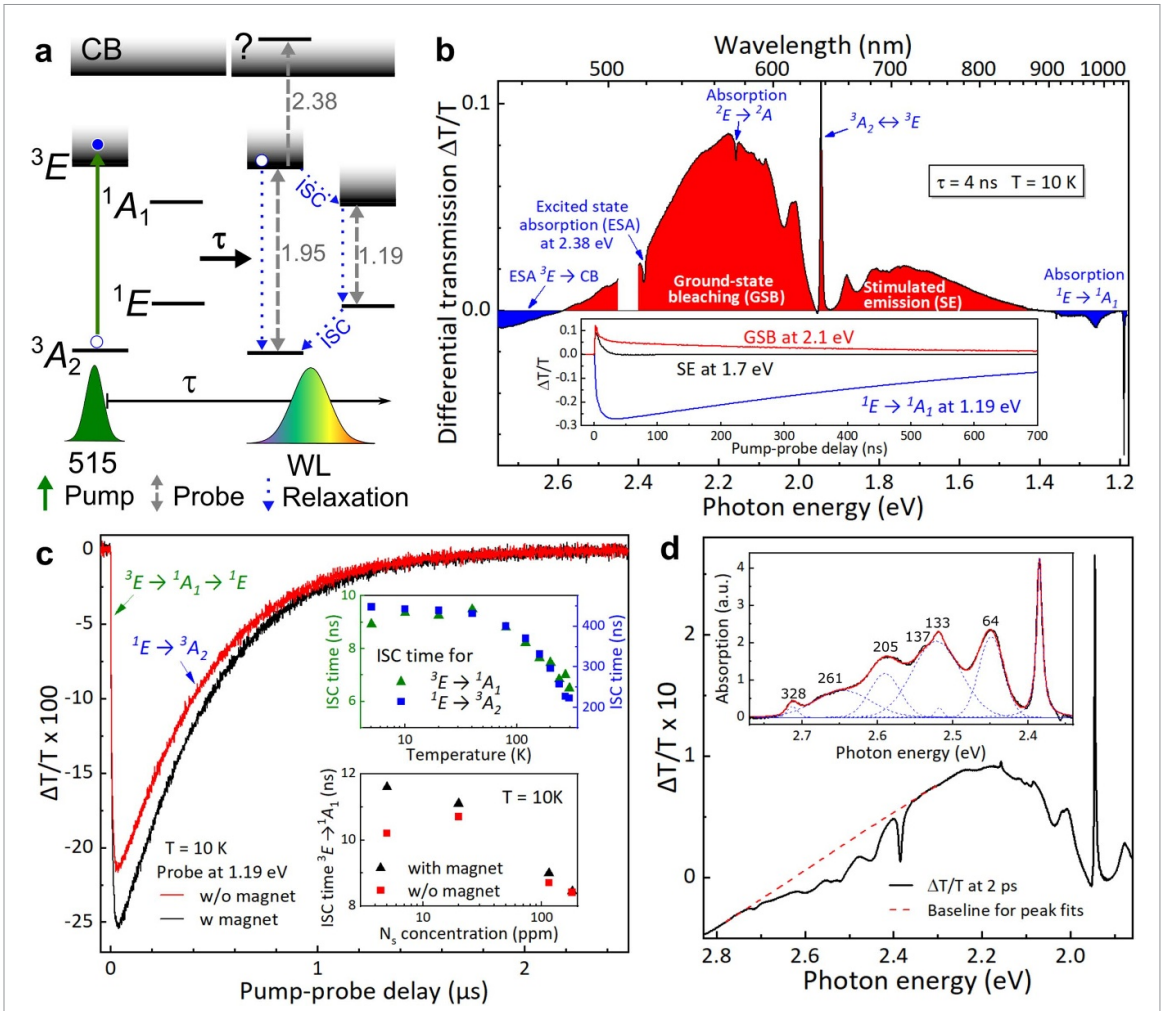


**Figure 1.** Dynamics of $NV^-$: (a) TA measurement scheme: solid lines denote excitation, blue-dashed arrows are relaxation pathways and grey-dashed lines relevant probe transitions, numbers are transition energies (eV); numbers below pulses denote wavelength (nm); (b) TA spectrum at pump-probe delay of 4 ns at 10 K. Inset: dynamics at certain probe energies. (c) $\Delta T/T$ dynamics of the $^1E \rightarrow {}^1A_1$ transition at 1.19 eV. Inset: temperature dependence of extracted ISC times and dependence of $^3E \rightarrow {}^1A_1$ ISC time on $N_s$ concentration. (d) $\Delta T/T$ at 2 ps, featuring ESA ZPL at 2.38 eV with PSB. Inset: baseline-corrected spectrum with peak fits. Numbers above peaks denote the energetic distance to ZPL (meV).

of this electronic state in the spin-singlet excitation experiments featured below, which strongly suggests it being a spin-triplet. Indications of this electronic state have been reported before in photoionization experiments [23]. This state, which ought to be resonant with the CB, has not been predicted by theory and its exact nature is thus unknown.

To study the singlet transition $^1E \leftrightarrow {}^1A_1$, we first excite the triplet transition with 515 nm, wait 15 ns, after which all $^3E$ population has either relaxed to $^3A_2$ or $^1E$, and then perform a pump-probe scan with 900 nm excitation (figure 2(a)). We observe the expected GSB of $^1E \rightarrow {}^1A_1$ at 1.19 eV and an ESA peak at 1.75 eV (figure 2(b)). As shown in the lower inset, this peak features a small PSB with two vibronic peaks. We attribute this ESA feature to the transition from $^1A_1$ to the so far only theoretically predicted third singlet state $^1E'$ [6, 9]. Both resonances decay exponentially with a constant of 130 ps, which implies that a) the lifetime of the $^1A_1$ state is 130 ps, in line with previous results [20], and b) that the newly observed ESA is indeed coming from an excited state accessed by $^1A_1$. As shown in figure 2(c), we observed transitions to even higher singlet states when probing towards the UV, as evidenced by ESA peaks at 2.78, 2.79 eV and 2.85 eV. The positive peak at 2.94 eV corresponds to the GSB of the $^1E \rightarrow {}^1E'$ transition ($= 1.19 + 1.75$ eV). Interestingly, this transition features a smaller adjacent peak, which is absent in the $^1E \rightarrow {}^1A_1$ and $^1A_1 \rightarrow {}^1E'$ transitions (supplementary figure 25). A reproducible sharp spectral feature of unknown origin is also present at 2.92 eV. Both resonances decay with the 130 ps population lifetime of $^1A_1$, consistent with our assignment of the peaks (figure 2(d)). The temperature dependencies of center photon energy and linewidth for all ZPLs can be found in supplementary figure 17.

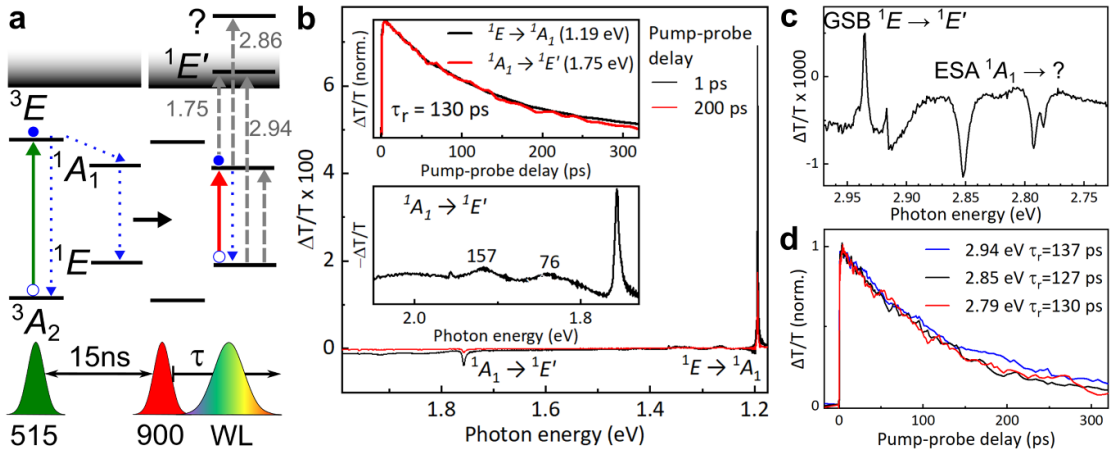


**Figure 2.** (a) Measurement scheme for the $^1E \rightarrow {}^1A_1$ transition. (b) $\Delta T/T$ spectra at two pump-probe delays, showing GSB of $^1E \rightarrow {}^1A_1$ at 1.19 eV and ESA of $^1A_1 \rightarrow {}^1E'$ at 1.75 eV. Insets: transients of both resonances and expanded view of $^1A_1 \rightarrow {}^1E'$ ESA spectrum; numbers are energy distance of vibronic peaks to ZPL (meV). (c) $\Delta T/T$ spectrum at 5 ps, showing GSB of $^1E \rightarrow {}^1E'$ at 2.94 eV and three additional ESA peaks, indicating singlet states above $^1E'$. (d) Transients of 2.94, 2.85 and 2.79 eV peaks that decay exponentially within ≈130 ps.

### 1.2. Electron transfer $NV^- \rightarrow NV^0$

For the next experiments, we pump at 620 nm to exclusively excite $NV^-$ (figure 3(a)), allowing to study $NV^-$ in samples with lower $N_s$ concentration that show $NV^0$ in equilibrium. We observe a rising appearance of absorption at 2.15 eV, see figure 3(b), indicating a bi-exponentially increasing population of the $^2E$ level of $NV^0$ (see inset). The absorption value at late pump-probe delays (e.g. 3 ns) scales linearly with pump fluence, which suggests that the process responsible for this absorption increase originates from $^3E$ (supplementary figure 19). The absorption value also scales with $N_s$ concentration, i.e. is larger in samples containing higher $N_s$ concentrations, see figure 3(c), where we plot the dynamics measured in samples with $N_s$ concentrations varying from 9 to 180 ppm. To properly compare these plots in terms of magnitude, we divided the absorption signal of $NV^0$ at 2.15 eV by the ZPL amplitude of the $NV^-$ triplet transition at $\tau = 0$, thereby normalizing for varying signal strengths across different samples. Our results combined with the linear pump fluence dependence strongly suggest that the observed dynamics originate from electron tunneling from $^3E$ to nearby $N_s$, which switches the charge state and creates $NV^0$ in its ground state $^2E$. We believe this electron transfer process is responsible for the commonly observed PL quenching and faster PL decay times in samples with high $N_s$ concentrations [11, 12]. This hypothesis is corroborated by figure 3(d), where we plot the measured $NV^-$ PL lifetime ($^3E \rightarrow {}^3A_2$) of our samples against the $NV^0$ absorption values at $\tau = 3$ ns, where one can observe a decreasing PL decay time for larger final $NV^0$ populations. The work by Manson *et al* [12] suggests that in the quasi-equilibrium established through photoexcitation, nearby NV-$N_s$ pairs are in the negative and positive charge state, respectively. That would imply that electron transfer would occur from $NV^-$ to $N^+$, temporally creating $NV^0$ and $N^0$, before back conversion occurs to $NV^-$ and $N^+$. We also measured the dynamics of this back-conversion process $NV^0 \rightarrow NV^-$ that proceeds on $\mu$s timescales (supplementary figure 22).

### 1.3. Intrinsic dynamics of $NV^0$

To study $NV^0$, we pump at 515 nm (figure 4(a)) on samples exhibiting a large fraction of $NV^0$ in equilibrium (samples S1 and S6, see supplementary figure 4 and table 1). Unlike $NV^-$, which we can exclusively excite with light between 580 nm and 640 nm, this is not possible with $NV^0$, and any pump event will also excite some fraction of $NV^-$. We verified that the measurements are related to $NV^0$ by comparing them to samples only containing $NV^-$ and measuring their decay time: the excited state lifetime of $NV^-$ is ≈10 ns, whereas it is 20 ns for $NV^0$ (supplementary figure 23). Figure 4(b) shows IR-TA spectra for three pump-probe delays up to 100 ns, where one can observe a broad ESA feature from 0.7 eV probe energy that increases towards the blue. A multitude of ESA resonances between 0.65 eV and 1.05 eV is also visible. As shown in the inset of figure 4(b), all features decay exponentially with a time constant of 20 ns, which matches the lifetime of $^2A_2$, and none of these features are present in $NV^-$-only samples (supplementary figure 23).

We observe the same resonances as GSB features in the UV, upshifted by 2.153 eV, which exactly matches the $NV^0$ ZPL energy. This is shown in figure 4(c), where we plot the UV TA data together with the ZPL-upshifted IR data. It is clear that the negative IR ESA peaks correspond in peak photon energy to the positive GSB peaks in the UV, albeit with different relative peak amplitudes. A pronounced ESA peak is

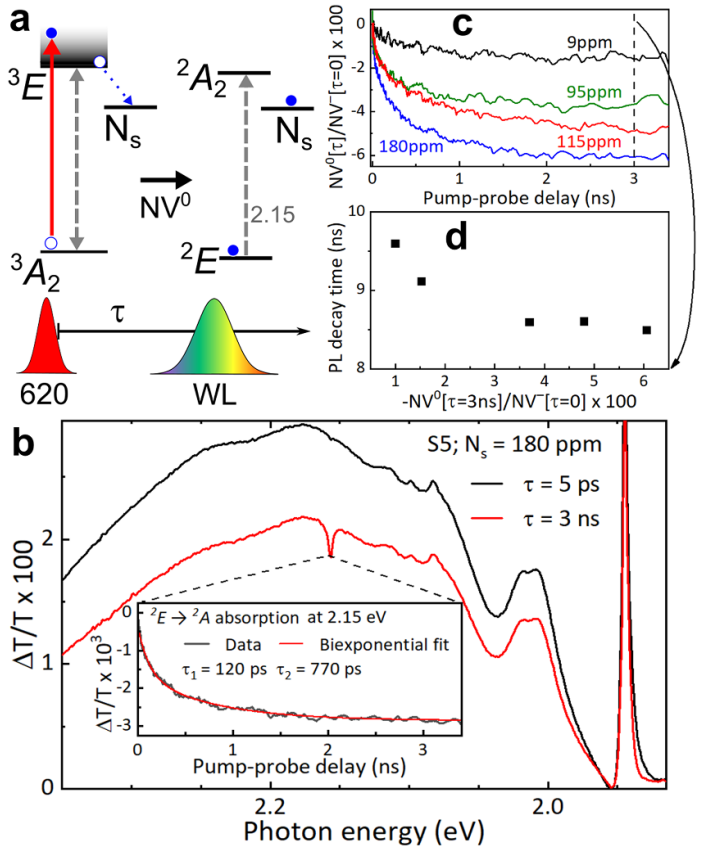


**Figure 3.** (a) Measurement scheme to probe conversion $NV^- \rightarrow NV^0$ mediated by electron transfer $^3E \rightarrow N_s$. (b) $\Delta T/T$ spectra at 5 ps and 3 ns, showing the appearance of absorption at 2.15 eV, indicative of populating $^2E$. Inset: dynamics of this process. (c) dynamics of $NV^0$ ZPL absorption increase for samples with varying $N_s$ concentrations and (d) the measured $NV^-$ PL lifetime as a function of normalized ZPL absorption amplitude at 3 ns.

visible at 2.94 eV that does not have an IR companion. It is the $^1E \rightarrow {}^1E'$ transition of $NV^-$ (figure 2(c)) that is activated by populating $^1E$ through two-photon ionization of $NV^0$ by the pump pulse, leading to charge conversion $NV^0 \rightarrow NV^-$ of some excited NV centers. We verified this through a pump power dependence that shows a second order relation for this peak but a linear dependence for all other peaks (supplementary figure 24). One can also recognize some of the UV TA peaks in steady-state absorption spectra, albeit with small amplitudes that make them easy to miss or misinterpret them as ZPLs from other spurious defects (supplementary figure 26). In this respect, the appearance of GSB peaks in the UV following $NV^0$ excitation at 515 nm unambiguously connects the according excited states to $NV^0$ since it proves them to share a common ground state, i.e. $^2E$ (see figure 4(a)). Note that PL excitation (PLE) spectra should in principle give similar results to our UV TA spectra, where one measures the $NV^0$ PL magnitude as a function of excitation photon energy, sweeping across the UV resonances. We are however not aware of any publication using this approach on $NV^0$.

We tentatively interpret the broad ESA in the IR to photoionization from $^2A_2$ into the valence band (VB) and its onset around 0.7 eV as the photoionization threshold. Such an excitation into the continuum should in the simplest case follow a power law, i.e. the absorption be proportional to the photon energy $E \propto a(E - E_0)^q$, where $a$ is a scaling factor, $E_0$ the photoionization threshold and $q$ the exponent. In the textbook case, $q$ should be 0.5 for a 3D semiconductor, however we find that $q = 0.33$ describes our data best, see blue plot in figure 4(c) (supplementary figure 27). The extracted ionization threshold $E_0$ at 0.717 eV is consistent with previous experimental and theoretical investigations [24]. We subtract the power-law-modeled baseline in a slightly modified version from our data as a basis for peak fits and plot the results in figure 4(d). We obtain eight Lorentzian resonances between 0.65 and 0.73 eV (see inset of 4(d)) and two resonances around 1.05 eV. The fitting parameters for these peaks and their UV counterparts can be found in supplementary table 3. Between 0.8 and 0.9 eV, dispersive resonances resembling Fano lineshapes are visible. These indicate transitions coupled to a continuum that would support our assignment of the broad ESA to excitation into the VB. That is somewhat in variance with the other resonances (also $NV^-$) which in terms of energy should be resonant with the VB ($NV^0$) or the CB ($NV^-$), however do not have Fano

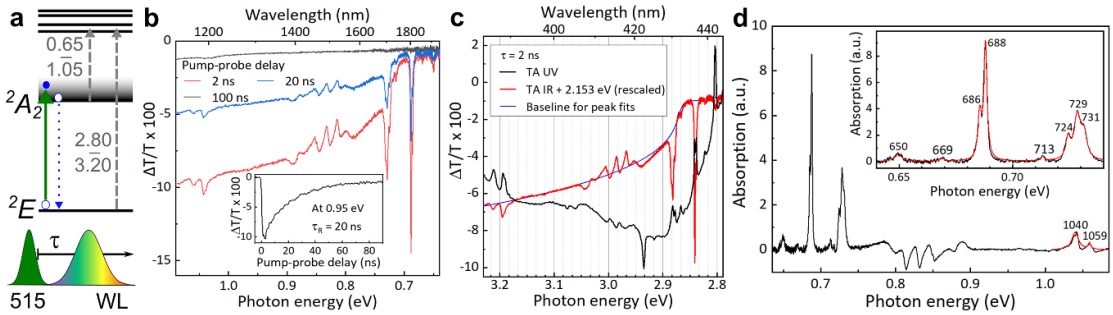


**Figure 4.** Dynamics of $NV^0$: (a) measurement scheme; (b) IR-TA spectra for three pump-probe delays. Inset shows exponential decay of ESA feature with 20 ns time constant. (c) UV-TA spectrum (black) and IR spectrum upshifted by $NV^0$ ZPL energy of 2.153 eV(red). Blue line: baseline following power law with coefficient 0.33. (d) Baseline-corrected IR-TA spectrum for visualization of ESA resonances. Inset shows a magnified part of 0.63–0.74 eV, with fits to Lorentzian peak model (red). Fitted center photon energies noted in meV.

lineshapes. Interestingly, in the case of the 2.38 eV transition (figure 1(d)), which appears as a Lorentzian peak with PSB and thus like a proper localized transition, previous experiments have shown this resonance leading to increased photoionization, i.e. it couples to the CB, which one naively would expect to show a more Fano-like lineshape as a consequence. Similar observations have been made in the neutral carbon vacancy in diamond (GR1), where a series of resonances (GR2-8) reminiscent of localized electronic transitions are also resonant with the VB, leading to hole current upon photoexcitation [25], a phenomenon that is not understood [26, 27].

As to the nature of the $NV^0$ excited states, there are two possibilities: additional NV localized states, similar to the ones we discovered for $NV^-$ and/or Rydberg states created by the bound exciton $NV^-$ + hole just below the ionization threshold of $NV^0$. Regarding the former, a few more spin-doublet states have been predicted by theory, which could thus explain some of the transitions, albeit not all [7, 28]. Concerning the Rydberg states, a very recent theoretical effort calculated the electronic structure of the $NV^-$ + hole bound exciton [8]. Interestingly, their results for the highest transitions, predicted to fall in the range between 430 and 445 nm, match our results very well. However, the lowest transitions 1s and 2p (between 450 and 475 nm), which should be the strongest, do not appear in our data.

In conclusion, by employing TA spectroscopy we monitored the relaxation dynamics of $NV^-$ and $NV^0$ centers after photoexcitation by transiently probing all relevant optical transitions from 400 to 2000 nm on timescales from fs to $\mu$s. We measured the electron tunneling dynamics from $^3E$ of $NV^-$ to nearby $N_s$ that leads to the well-known effect of PL quenching, for the first time probing the underlying dynamics. We showed that we can directly probe the singlet relaxation pathway of $NV^-$ and extract all relevant kinetic rates. This approach will be applicable to other defects where ISC-driven relaxation pathways are known to exist, yet have not been observed optically [29]. For both NV charge states we discover a large number of hitherto unknown electronic states. In the case of $NV^-$, we unambiguously proved the existence of NV electronic states that are resonant with the CB. Transitions to these states can potentially be exploited to enhance ionization rates and thus the spin contrast in magnetometry schemes where the photocurrent is detected instead of PL [9, 10]. For $NV^0$, our results show an intricate mixture of localized and bound-to-continuum transitions as evidenced by Lorentzian and Fano resonances, respectively. Some of these transitions could be the first experimental verification of the only very recently predicted Rydberg states from the bound exciton $NV^-$ + hole [8]. The unique capability of TA spectroscopy to probe these excited state transitions both from the $NV^0$ ground state $^2E$ and first excited state $^2A_2$ revealed that the absorption cross sections vary greatly between both scenarios, providing clues for the nature of the new excited states. More work is required to shed light on these issues. We are preparing spectrally-resolved photoionization experiments that will be particularly insightful regarding the rich excited state manifold of $NV^0$: is the broad ESA due to continuum excitation and are the sharp resonances exciton Rydberg states and/or localized electronic states of $NV^0$? *Ab initio* simulations are also under way to support our experimental findings.

## 2. Methods

The experimental TA setups use an ultrafast fiber-based Ytterbium laser emitting 150 fs long pulses with a center wavelength of 1030 nm laser (Amplitude Tangerine SP) at a tunable repetition rate of up to 40 MHz. Experiments were performed at various repetition rates, but were usually kept below 10 kHz. The output of the laser is separated into three different paths: the first path ('OPA path') is fed into a home-built optical

parametric amplifier (OPA), which generates tunable output at 650–2500 nm. The second path ('NOPA path') is directed into a noncollinear OPA (AG-Riedle NOPA Rainbow), which is generating pulses between 620 nm and 950 nm. Finally, the third path ('second harmonic generation (SHG) path') goes directly through a frequency-doubling BBO crystal, generating pulses at 515 nm. All samples are mounted inside a closed-cycle Helium cryostat (Advanced Research Systems ARS-10HW) for cryogenic measurements. Two TA setups are used: for fs–ns timescales and ns–ms timescales.

For the fs–ns TA setup, the SHG and/or NOPA paths are utilized as the pump pulses, while the OPA path is used as a source for white light (WL) generation to create a broadband white-light (WL) probe by focusing into a c-cut sapphire window. Before entering the TA setup, the pump pulse transmission is mechanically modulated by an optical chopper, whose phase is synchronized with the laser output. Pump and probe beams are focused onto the sample, ensuring proper spatial overlap. The probe beam, after interacting with the sample, is recollimated and then imaged on to a line camera (Teledyne e2V Octoplus for VIS-NIR/UV and Xenics Manx R 2048 for IR).

For the ns–ms TA setup, the SHG or NOPA paths are employed as the pump and instead of a second pulsed probe, a continuous wave (CW) incoherent broadband WL source (XWS-30, ISTEQ BV) is used as the probe. The transmitted broadband WL through the sample is passed through a monochromator and measured with a fast photodiode (PD). The output signal of the PD is amplified and recorded with a digitizer that is synchronized with the pump pulse, resulting in time-resolved pump-induced differential transmission. The measurement duration can be extended up to milliseconds or seconds employing this approach with a time resolution of 1 ns, which is defined by the rise and fall time of the electronic instruments including the PD, amplifier, and digitizer. More information on the experimental methods can be found in supplementary section 1.1.

## Data availability statement

The data cannot be made publicly available upon publication because they are not available in a format that is sufficiently accessible or reusable by other researchers. The data that support the findings of this study are available upon reasonable request from the authors.

## Acknowledgments

We are grateful to Neil Manson for sample provisions and many discussions. We acknowledge Jürgen Worm, Marc-Jan van Zadel and Florian Gericke for technical support. For insightful discussions we thank Audrius Alkauskas, Gergő Thiering, Lukas Razinkovas, Carlos Meriles, Chris van de Walle, Mark Turiansky and Marcus Doherty. We thank Mischa Bonn for comments on the manuscript. R U is grateful to Zhi-Heng Loh for support with preliminary measurements. We acknowledge funding by the Max-Planck Society.

## Author contributions

M-T L and A T Y contributed equally to this work. R U conceived and supervised the project. M-T L and A T Y performed the measurements. M-T L, A T Y and R U analyzed the data. R U wrote the manuscript with input from all authors.

## Conflict of interest

The authors declare no competing interests.

## ORCID iDs

Ali Tayefeh Younesi https://orcid.org/0000-0002-5156-5226
Ronald Ulbricht https://orcid.org/0009-0001-3370-5520

## References

[1] Rondin L, Tetienne J-P, Hingant T, Roch J-F, Maletinsky P and Jacques V 2014 Magnetometry with nitrogen-vacancy defects in diamond *Rep. Prog. Phys.* **77** 056503
[2] Barry J F, Schloss J M, Bauch E, Turner M J, Hart C A, Pham L M and Walsworth R L 2020 Sensitivity optimization for NV-diamond magnetometry *Rev. Mod. Phys.* **92** 015004
[3] Ashfold M N R, Goss J P, Green B L, May P W, Newton M E and Peaker C V 2020 Nitrogen in diamond *Chem. Rev.* **120** 5745–94
[4] Shinei C, Miyakawa M, Ishii S, Saiki S, Onoda S, Taniguchi T, Ohshima T and Teraji T 2021 Equilibrium charge state of NV centers in diamond *Appl. Phys. Lett.* **119** 254001

[5] Doherty M W, Manson N B, Delaney P, Jelezko F, Wrachtrup J and Hollenberg L C L 2013 The nitrogen-vacancy colour centre in diamond *Phys. Rep.* **528** 1–45
[6] Gali A 2019 *Ab initio* theory of the nitrogen-vacancy center in diamond *Nanophotonics* **8** 1907–43
[7] Pfäffle W, Antonov D, Wrachtrup J and Bester G 2021 Screened configuration interaction method for open-shell excited states applied to NV centers *Phys. Rev.* B **104** 104105
[8] Chen Y, Oberg L, Flick J, Lozovoi A, Meriles C A and Doherty M W 2024 Semiempirical *ab initio* modeling of bound states of deep defects in semiconductor quantum technologies *Phys. Rev.* B **109** L201115
[9] Wirtitsch D, Wachter G, Reisenbauer S, Gulka M, Ivády V, Jelezko F, Gali A, Nesladek M and Trupke M 2023 Exploiting ionization dynamics in the nitrogen vacancy center for rapid, high-contrast spin and charge state initialization *Phys. Rev. Res.* **5** 013014
[10] Bourgeois E, Gulka M and Nesladek M 2020 Photoelectric detection and quantum readout of nitrogen-vacancy center spin states in diamond *Adv. Opt. Mater.* **8** 1902132
[11] Capelli M *et al* 2022 Proximal nitrogen reduces the fluorescence quantum yield of nitrogen-vacancy centres in diamond *New J. Phys.* **24** 033053
[12] Manson N B, Hedges M, Barson M S J, Ahlefeldt R, Doherty M W, Abe H, Ohshima T and Sellars M J 2018 $NV^{-}$–$N^{+}$ pair centre in 1b diamond *New J. Phys.* **20** 113037
[13] Robledo L, Bernien H, Sar T V D and Hanson R 2011 Spin dynamics in the optical cycle of single nitrogen-vacancy centres in diamond *New J. Phys.* **13** 025013
[14] Acosta V M, Jarmola A, Bauch E and Budker D 2010 Optical properties of the nitrogen-vacancy singlet levels in diamond *Phys. Rev.* B **82** 201202(R)
[15] Smallwood C L, Ulbricht R, Day M W, Schröder T, Bates K M, Autry T M, Diederich G, Bielejec E, Siemens M E and Cundiff S T 2021 Hidden silicon-vacancy centers in diamond *Phys. Rev. Lett.* **126** 213601
[16] Younesi A T and Ulbricht R 2022 Broadband transient absorption spectroscopy using an incoherent white-light source as probe *Opt. Express* **30** 38896–906
[17] Liu A, Cundiff S T, Almeida D B and Ulbricht R 2021 Spectral broadening and ultrafast dynamics of a nitrogen-vacancy center ensemble in diamond *Mater. Quantum Technol.* **1** 025002
[18] Ulbricht R, Dong S, Chang I-Y, Mariserla B M K, Dani K M, Hyeon-Deuk K and Loh Z-H 2016 Jahn-Teller-induced femtosecond electronic depolarization dynamics of the nitrogen-vacancy defect in diamond *Nat. Commun.* **7** 13510
[19] Ulbricht R, Dong S, Gali A, Meng S and Loh Z-H 2018 Vibrational relaxation dynamics of the nitrogen-vacancy center in diamond *Phys. Rev.* B **97** 220302(R)
[20] Ulbricht R and Loh Z-H 2018 Excited-state lifetime of the $NV^{-}$ infrared transition in diamond *Phys. Rev.* B **98** 094309
[21] Goldman M L, Sipahigil A, Doherty M, Yao N, Bennett S, Markham M, Twitchen D, Manson N, Kubanek A and Lukin M 2015 Phonon-induced population dynamics and intersystem crossing in nitrogen-vacancy centers *Phys. Rev. Lett.* **114** 145502
[22] Shinei C, Masuyama Y, Miyakawa M, Abe H, Ishii S, Saiki S, Onoda S, Taniguchi T, Ohshima T and Teraji T 2022 Nitrogen related paramagnetic defects: decoherence source of ensemble of $NV^{-}$ center *J. Appl. Phys.* **132** 214402
[23] Beha K, Batalov A, Manson N B, Bratschitsch R and Leitenstorfer A 2012 Optimum photoluminescence excitation and recharging cycle of single nitrogen-vacancy centers in ultrapure diamond *Phys. Rev. Lett.* **109** 097404
[24] Aslam N, Waldherr G, Neumann P, Jelezko F and Wrachtrup J 2013 Photo-induced ionization dynamics of the nitrogen vacancy defect in diamond investigated by single-shot charge state detection *New J. Phys.* **15** 013064
[25] Clark C D, Parsons B J and Vermeulen L A 1979 Photo-Hall effect measurements in irradiated diamond *J. Phys. C: Solid State Phys.* **12** 2597
[26] Stoneham A 1992 Theoretical status of diamond and its defects, excited states and atomic motion *Mater. Sci. Eng.* B **11** 211–8
[27] Mainwood A 1978 Calculation of linewidths of the GR2-8 transitions in diamond in a model where the energy levels are within the valence band *J. Phys. C: Solid State Phys.* **11** L449
[28] Ranjbar A, Babamoradi M, Heidari Saani M, Vesaghi M A, Esfarjani K and Kawazoe Y 2011 Many-electron states of nitrogen-vacancy centers in diamond and spin density calculations *Phys. Rev.* B **84** 165212
[29] Dong W, Doherty M W and Economou S E 2019 Spin polarization through intersystem crossing in the silicon vacancy of silicon carbide *Phys. Rev.* B **99** 184102